Front. Earth Sci. 2020, 14(2): 344–359
https://doi.org/10.1007/s11707-019-0781-9

RESEARCH ARTICLE

# Variabilities of carbonate $\delta^{13}C$ signal in response to the late Paleozoic glaciations, Long'an, South China

**Bing YANG[1,2], Xionghua ZHANG (✉)[1], Wenkun QIE[3], Yi WEI[4], Xing HUANG[3], Haodong XIA[2]**

1 Faculty of Earth Sciences, China University of Geosciences, Wuhan 430074, China
2 Cores and Samples Centre of Natural Resources, Langfang 065201, China
3 State Key Laboratory of Palaeobiology and Stratigraphy, Nanjing Institute of Geology and Palaeontology and Center for Excellence in Life and Palaeoenvironment, Chinese Academy of Sciences, Nanjing 210008, China
4 School of Safety Engineering, North China Institute of Science and Technology, Langfang 065201, China



**Abstract** An integrated study of biostratigraphy, microfacies, and stable carbon isotope stratigraphy was carried out on the late Famennian–early Asselian carbonates of the Long'an section in Guangxi, South China. Stable carbon isotope studies in the Long'an section have revealed four major positive shifts of $\delta^{13}C$ values in the Carboniferous strata in South China. The first shift occurred in the *Siphonodella dasaibaensia* zone in the Tournaisian, with an amplitude of 4.19‰. The second shift occurred near the Visean/Serpukhovian boundary, with an amplitude of 2.63‰. The third shift occurred in the Serpukhovian, with an amplitude of 3.95‰. The fourth shift occurred in the Kasimovian, with an amplitude of 3.69‰. Furthermore, there were several brief positive $\delta^{13}C$ shifts during the late Famennian to early Tournaisian. All of these shifts can be well correlated globally, and each corresponds to sea-level regressions in South China and Euro-America, indicating increases in ocean primary productivity and global cooling events. Chronologically, the four major positive excursions of $\delta^{13}C$, together with several brief positive $\delta^{13}C$ shifts that were observed during the late Famennian to the early Tournaisian, correspond to the well-accepted Glacial I, II, and III events.

**Keywords** carbon isotopes, Late Paleozoic Ice Age, Carboniferous, sea-level changes, global climate variation

## 1 Introduction

The Carboniferous period witnessed large changes in paleogeography, paleoclimate, and paleooceanic environments. Laurussia collided and merged with Gondwana, causing the formation of Pangaea, and the global ocean current circulatory system and thermal transfer system changed significantly (Saltzman, 2003). Furthermore, flourishing land vegetation enhanced the flux of terrestrial weathering, resulting in a rise in primary productivity and organic carbon burial and, ultimately, a decline in atmospheric $CO_2$ levels and a cooler climate (Mii et al.,1999; Saltzman, 2003 and 2002). Correspondingly, an ice age occurred in the Late Paleozoic (Mii et al., 2001; Lin et al., 2002). The glacial dynamics are documented by the distributions of till and tillite deposits at high latitudes (Frakes et al., 1992; Caputo and Crowell, 1985). However, global correlation of glaciation is very difficult due to sparse age data and a lack of age-diagnostic index fossils (Smith and Read, 2000). Multiple proxies, including carbon isotopes from bulk carbonates, well-preserved brachiopod shells, oxygen isotopes of brachiopods, and conodonts (Mii et al., 1999; Saltzman et al., 2000; Saltzman, 2003; Smith and Read, 2000; Grossman et al., 2008; Buggisch et al., 2008), cyclostratigraphic data, and sea-level fluctuations, have been used to constrain Late Paleozoic glaciations (Crowell, 1978; Veever and Powell, 1987). Some researchers proposed three episodes of glaciation based on three profound positive shifts of $\delta^{13}C$ and $\delta^{18}O$ in the Tournaisian, Serpukhovian, and the Kasimovian on the US Midcontinent and Russian Platform (Saltzman et al., 2000; Mii et al., 2001; Grossman et al., 2008), and the corresponding relationships between Late Paleozoic ice ages and carbon isotopes were established.

In the past, studies of sea-level changes in the mid-low latitudes, cyclostratigraphic studies, and carbon-oxygen isotope studies of the Late Paleozoic, have mainly been conducted in North America and Europe (Bruckschen et al., 1999; Mii et al., 2001; Saltzman, 2003; Wynn and Read, 2007; Buggisch et al., 2008; Grossman et al., 2008).

Received March 19, 2019; accepted July 16, 2019

E-mail: zhangxh@cug.edu.cn

In recent years, research on Carboniferous sequence stratigraphy, cyclostratigraphy and stable carbon isotopes in South China have become important topics. For example, Wang et al. (2013) comprehensively discussed the Gondwanan ice age, based on cyclostratigraphic and sedimentological research in South China. Liu et al. (2017) recognized seven cooling and two warming pulses in the mid-Pennsylvanian to the middle Guadalupian interval, based on sedimentological and stable carbon isotope research in South China. Chen et al. (2016) proposed an initial buildup of Gondwanan ice sheets in the Visean-Serpukhovian boundary interval, based on sedimentological and high-resolution $\delta^{13}C$ research in South China. Many carbon isotope studies have been conducted in the Carboniferous-Permian sections, which are located in southern China, such as the Dushan section, the Naqing section, the Zongdi section, the Yashui section, the Dianzishang section, the Narao section, the Luokun section in Guizhou, the Gongchuan section in Sichuan Province, the Fenghuangshan section in Anhui, the Kongshan section in Jiangsu, the Long'an section, and the Baping section in Guangxi. However, these studies were either measured from the short sections or at very low resolution (Li et al., 1996; Lin et al., 2002; Qie et al., 2007 and 2010; Buggisch et al., 2011; Chen et al., 2016; Liu et al., 2017). Until now, not a complete and successive Carboniferous carbon isotopic succession has been there from a single region in China. Qie et al. (2010) reconstructed the Late Paleozoic ice age with carbon isotope studies and identified a total of three ice age episodes in the Tournaisian to Bashkirian interval and the Visean to Bashkirian interval in respectively the Long'an section and the Baping section. However, due to low sampling resolution, except for the first episode, most glaciation events are consistent with the positive shifts only caused by minor fluctuations. As the glaciation event in the Pennsylvanian was not mentioned in that paper, the overall appearance of the Late Paleozoic ice age has not been fully discussed.

Here, detailed carbon isotope records from the Long'an section, South China were presented 1) to discuss the relationship between sea-level fluctuations and carbon isotope changes during the Carboniferous and 2) to be combined with comparisons of the records from Euro-American areas to investigate the Carboniferous sedimentological and carbon isotope responses with respect to Late Paleozoic ice age events.

## 2 Geological setting

During the Carboniferous, the South China Plate was located in the southern hemisphere near the equator (Fig. 1; Saltzman, 2003). During the Mississippian, the Yangtze ancient land was connected to the Cathaysia ancient land, and terrestrial sedimentation was widespread along the marginal areas while carbonate platforms were less distributed in Yunnan, Guizhou and Guangxi. During the Pennsylvanian, the ancient land was greatly reduced while the carbonate platform areas greatly increased (Feng et al., 1998).

The Long'an section, located on the Yunnan-Guizhou-Guangxi-Hunan carbonate platform, far from the ancient land (Fig. 1), is located approximately 3 km south of Dujie Town, South China. The Carboniferous strata are composed of Mississippian deposits, including the Rongxian, Long'an, Du'an Formations, and Pennsylvanian deposits, including the Dapu, Huanglong, and Maping Formations. The Rongxian Formation mainly consists of lime mudstone. The Long'an Formation mainly consists of bioclastic packstone, and lime mudstone interbedded with chert nodules. The Du'an Formation consists of wackestone and bioclastic packstone in the lower part and bioclastic grainstone and algal bondstone in the upper part. The Dapu Formation mainly consists of dolomite, bioclastic grainstone and partly dolomite limestone. The Huanglong Formation mainly consists of bioclastic grainstone, interbedded with dolomite limestone and bioclastic packstone in the lower part and bioclastic grainstone and bioclastic packstone in the upper part. The Maping Formation consists of bioclastic grainstone, bioclastic intraclast grainstone and a few oolitic grainstones.

## 3 Methods

We collected 690 unweathered samples for biostratigraphy, microfacies, and stable isotope analyses in the Long'an section, and carefully avoided Calcite veins and recrystallized areas. A microfacies analysis based on the detailed study of almost 214 thin sections has been performed for the Long'an section and followed the Flügel (2010) classification, we identified 11 microfacies. For biostratigraphy, 150 thin sections were produced, and the identification of Fusulinids and smaller foraminifers was conducted at Key Laboratoryof Biogeology and Environmental Geology of Ministry of Education, China University of Geosciences.

Carbon isotope values are likely to be preserved during the diagenetic processes that typically affect marine carbonates, and are widely used to investigate evolutionary trends of carbon isotopes of ancient ocean (Saltzman et al., 2000; Buggisch et al., 2008). Carbon and oxygen isotopic rations were measured from 326 bulk limestone samples from the Long'an section. Carbonate samples (1–5 g) were carefully collected to avoid cracks, calcite veins, and bioclasts. All of the samples were crushed to less than 200 mesh before carbon and oxygen isotope measurement. The samples were reacted with 100% phosphoric acid, and the resulting gas was transferred to

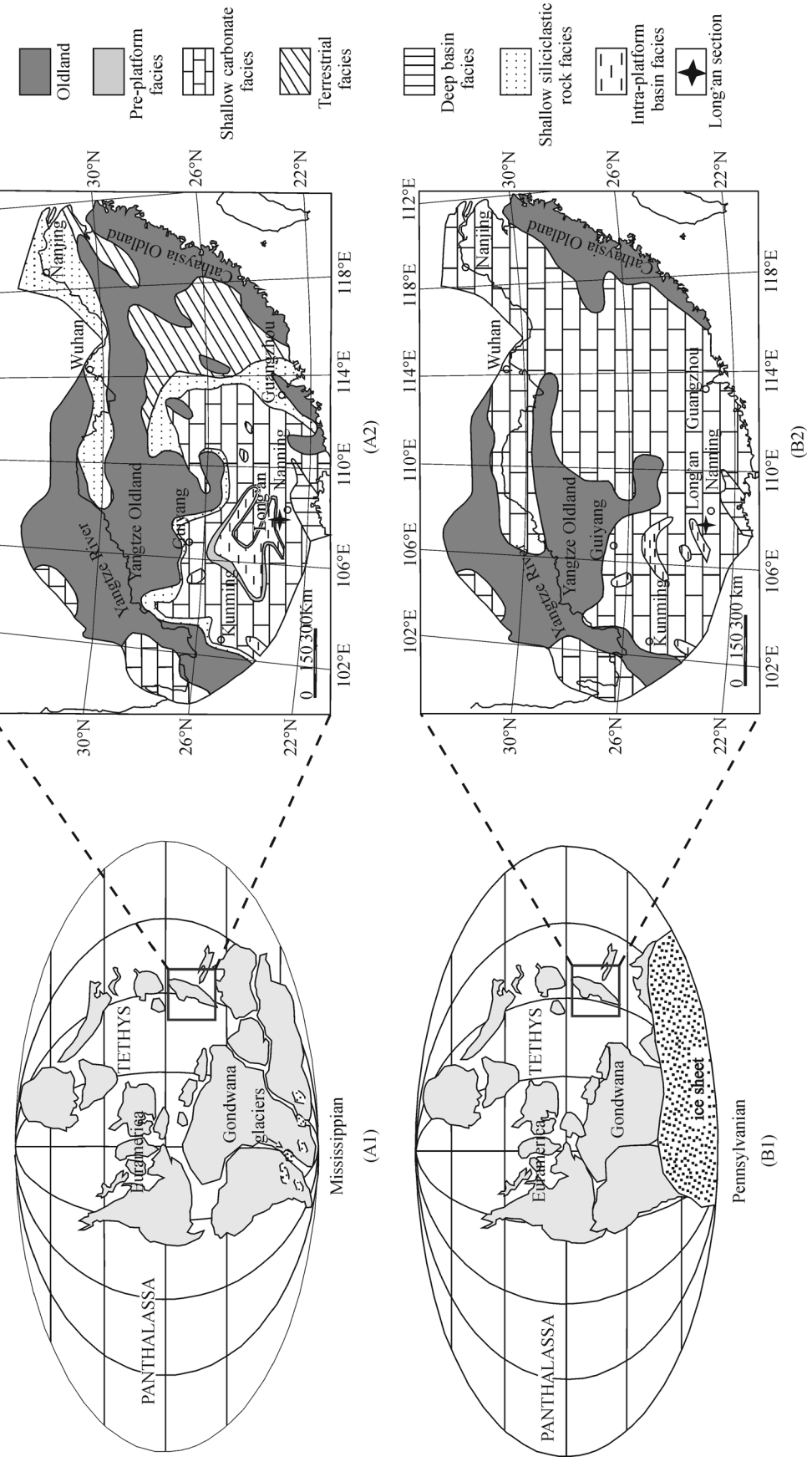


**Fig. 1** Reconstruction map of Carboniferous paleogeography. (A1) (B1) The global Carboniferous paleogeographic reconstruction map, modified after Saltzman (2003); (A2) (B2) The Carboniferous lithofacies-paleogeography map of south China, modified after Feng et al. (1998).

a Finnigan MAT 253 mass spectrometer. The isotopic standard reference material GBW-04416 ($\delta^{13}C = 1.61‰$, $\delta^{18}O = 11.59‰$) served as the international standard sample. The $\delta^{13}C$ and $\delta^{18}O$ values were reported in permil relative to international V-PDB (Vienna Peedee belemnite), and the precision of the carbon and oxygen isotope measurements was better than ±0.1‰. The experiment was conducted in the State Key Laboratory of Geological Process and Mineral Resources, China University of Geosciences (Wuhan).

## 4 Results

### 4.1 Biostratigraphy

The biostratigraphic framework of the Long'an section is based on conodonts, foraminifera and fusulinids. Nine international standard conodont zones were established in the Long'an Formation at the base of section, and in ascending order, these zones are: Lower *Siphonodella praesulcata* zone, Middle *Siphonodella praesulcata* zone, Upper *Siphonodella praesulcata* zone, *Siphonodella homosimplex, Siphonodella sinensis*, *Siphonodella dasaibaensia* zone, *Polygnathus communis carina*, *Gnathodus cuneiformis*, and *Polygnathus communis porcatus* (Qie et al., 2014 and 2015), indicating late Famennian to Tournaisian ages.

The age of the lower Du'an Formation, based on foraminifera, has been as placed into the Visean interval (Kuang et al., 1999).

Abundant smaller foraminifera and a few fusulinids were found in the upper Du'an Formation in beds 42 to 51 (Fig. 2). Among which, the *Janischewskina* sp., *Cribrospira panderi*, *Earlandia vulgaris* occurred in the upper Visean to the lower Serpukhovian, but *Eostaffella* was the important genus in the Serpukhovian (Kabanov et al., 2016). We place the boundary of the Visean and Serpukhovian stages in bed 42.

Fusulinids from the Dapu to Maping Formations can be divided into six fusulinid genozones: the *Pseudostaffella* zone, *Profusulinella* zone, *Fusulinella-Fusulina* zone, *Triticites* zone, *Quasifusulina* zone and *Pseudoschwagerina* zone (Fig. 3).

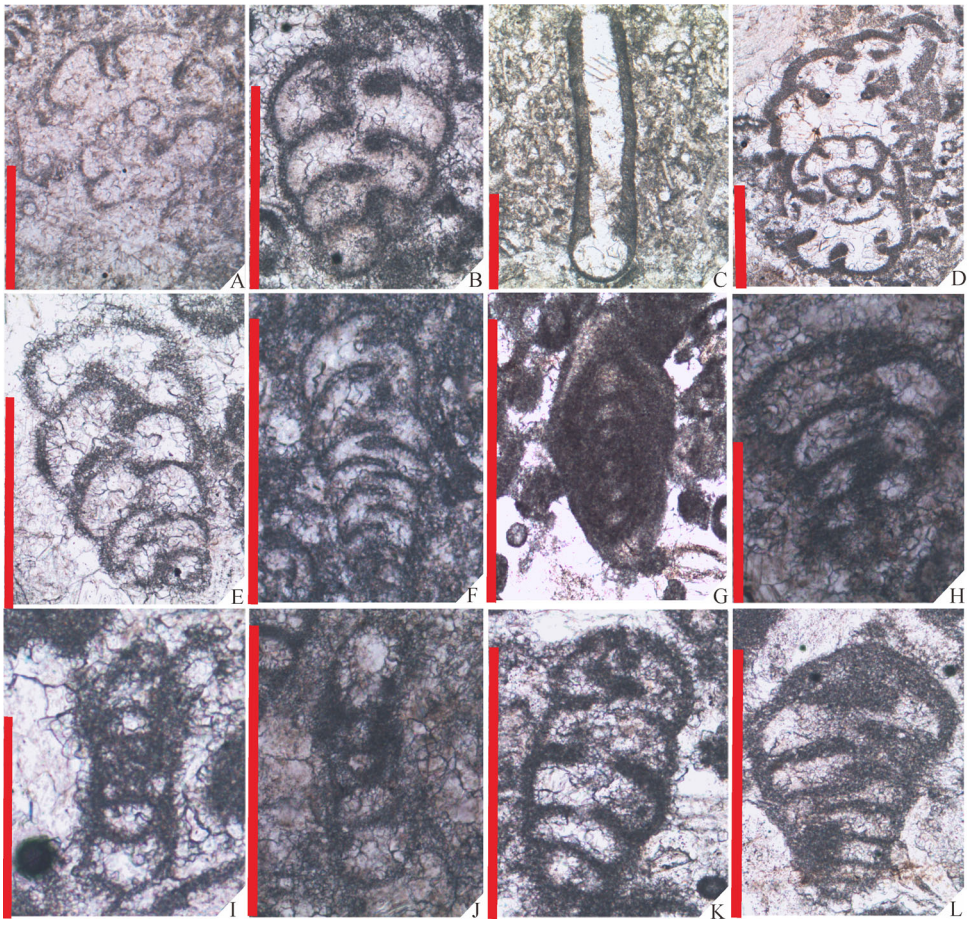


**Fig. 2** Foraminifera from the upper Du'an Formation (beds 42–51). A. *Janischewskina* sp.; B. *Koskinotextularia* sp.; C. *Earlandia vulgaris*; D. *Cribrospira panderi*; E, H. *Consobrinella consobrina*; F. *Palaeotextularia* sp.; G. *Eostaffella* sp.; I. *Mediocris breviscula*; J. *Forschia* sp.; K. *Cribrostomum* sp.; L, *Palaeotextularia gibbosa minima.* (A–H, J–L Scale bars = 1 mm; I Scale bars = 0.5 mm).

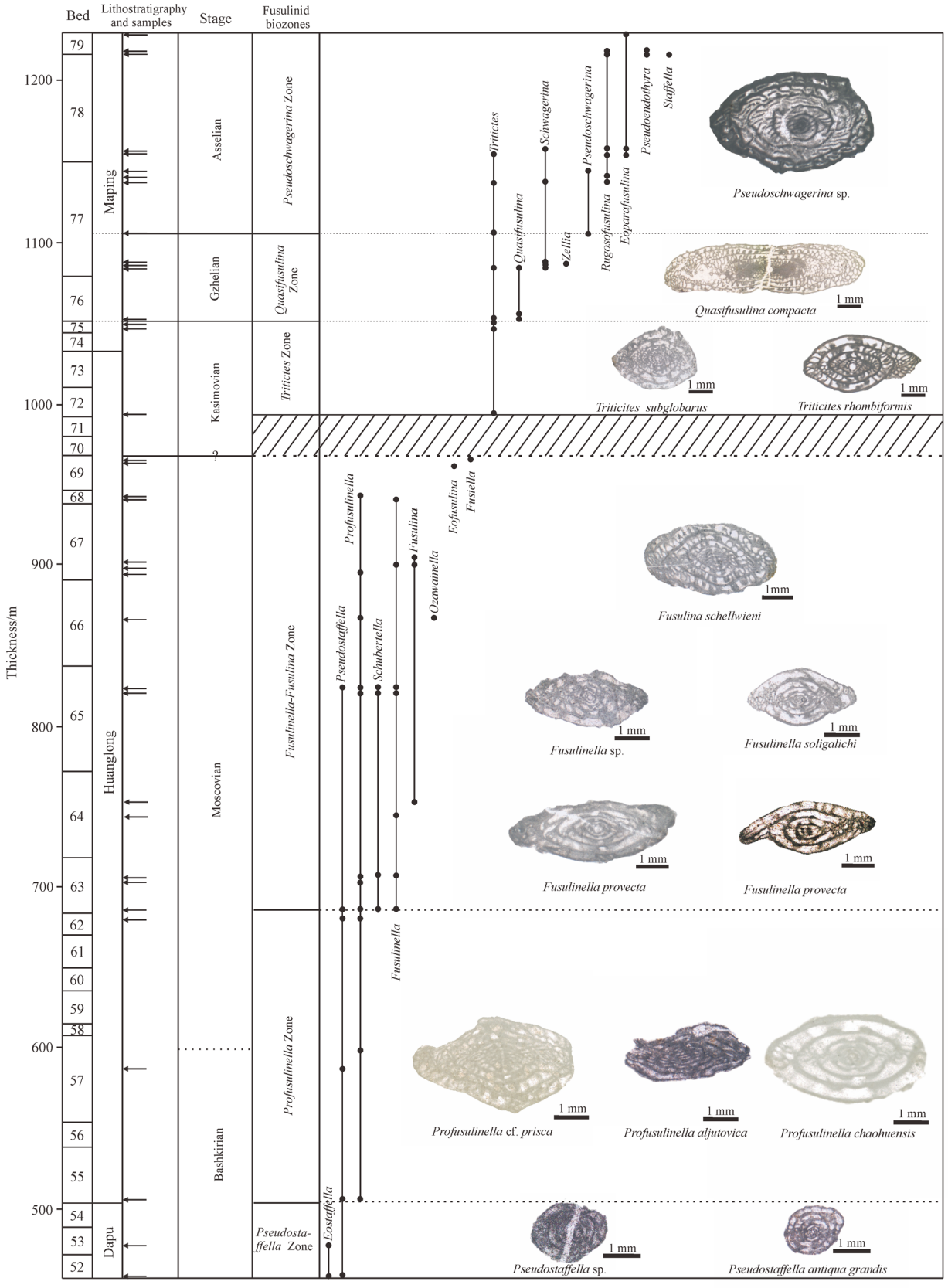


**Fig. 3** Range chart showing stratigraphic distributions of fusulinids and biochronology in the Bashkirian through Asselian in the Long'an section.

The *Pseudostaffella* zone is distributed in the Dapu Formation (beds 52–54). In the Guizhou area, the genus *Pseudostaffella* first occurs in the *Pseudostaffella antiqua-P. antiqua posterior* zone, which defines the early Bashikirian (Zhang et al., 2010); the basal Huanglong Formation (beds 55–62) is attributed to the *Profusulinella* zone, and the genus *Profusulinella* first occurs in bed 55. In addition, *Profusulinella aljutovica* first occur in the upper part of bed 57, which can be used as an auxiliary marker for the Bashikirian-Moscovian boundary (Ma et al., 2013); we place the boundary in the upper part of bed 57. The middle Huanglong Formation (beds 63–69) is attributed to the *Fusulinella-Fusulina* zone, and the genus *Fusulinella* first occurs in bed 63. The genus *Fusulinella* flourished during the Dalaun in South China, which is equivalent to the mid-late Moscovian as an international stratigraphic subdivision (Zhang et al., 2010). This genus occurs in the late Carboniferous and is widely reported in Guangxi, Guizhou and Fujian (Yang, 1989; Shi et al., 2009; Li et al., 2011). The genus *Fusulina* commonly occurs in the late Moscovian in Guangxi and Guizhou (Shi et al., 2009). As dolomitization exists in beds 70–71, these fusulinid fossils do not appear in these beds. The genus *Triticites* first occurs in bed 72, including *Triticites subglobarus*, *Triticites rhombiformis*, *Triticites* sp. etc. This genus commonly occurs in the upper Kasimovian and Gzhelian in South China and in the Russian Platform. For the transition of the Kasimovian and Gzhelian stages, the index genus Rauserites is scarce, but *Quasifusulina*, a large genus with a thick axial filling, first occurs near this boundary (Ueno et al., 2013; Okuyucu, 2013). We place this boundary at the sharp change from packstones to mudstones in bed 76, just below the FAD of *Quasifusulina*. The upper Maping Formation (beds 77–79) is attributed to the *Pseudoschwagerina* zone. *Pseudoschwagerina* sp., which first occurs in the middle part of bed 77, is commonly found in the early Permian in South China (Zhou, 1991). *Pseudoschwagerina* is the index genus for the early Permian. We place the boundary below the FAD of *Pseudoschwagerina* sp.

### 4.2 Microfacies analysis

Eleven microfacies were identified in the Long'an section across the Famennian to Asselian interval (Table 1). Records of texture, dominant components, interpretations, and stratigraphic distributions are presented here.

**Mf1: Lime mudstone**

Lime mudstone is mainly distributed in the Long'an Formation, the matrix of which is mainly mud crystals and is occasionally interbedded with chert nodules. The grain concentrations are less than 10% and are mainly bioclasts, including calcareous algae, ostracods, brachiopods, gastropods, and calcispheres (Figs. 4(a) and 4(b)). This indicates an inner shelf facies with low energy below the storm weather wave base.

**Mf2: Oolitic grainstone**

Oolitic grainstone is mainly distributed in the Du'an Formation. The grains are mainly composed of oolitic and echinodermata clasts, which are cemented by sparry calcite. Most of the oolites are well-sorted and concentric with small diameters (0.2–0.6 mm), some are algae ooids (Fig. 4(c)). This microfacies therefore indicates a platform margin sand shoal facies, which formed in a normal marine setting within the fair-weather wave action zone.

**Mf3: Bioclastic grainstone**

Bioclastic grainstone is mainly distributed in the Huanglong Formation and Maping Formation. Accounting for more than 50%, bioclasts are cemented by sparry calcite. These bioclasts mainly include calcareous algae, crinoid stem clasts, smaller foraminifera, fusulinid, etc. (Fig. 4(d)). This microfacies indicates a bioclastic shoal facies, which formed in a normal marine setting within a fair-weather wave action zone.

**Mf4: Fenestral boundstone**

Fenestral boundstone is mainly distributed in the Du'an Formation. Fenestral boundstone mostly consists of cyanobacteria symbiotic with lamellar algal boundstone. The irregularly distributed cavities are 0.05–0.5 mm in diameter and are filled with sparry calcite with few fossils (Fig. 4(e)). All petrographic features point to a high energy

**Table 1** Summary of the characteristics of the five major facies associations of the Long'an section

| Facies | Microfacies | Beds |
|---|---|---|
| Restricted platform facies | Mf6, Mf9, Mf10, Mf11 | 27,34,35,36,46,54,55,56,58,59, 62,64,70,71,73,77 |
| Open platform facies | Mf6, Mf7, Mf8, Mf9 | 5,6,7,11,13,22,23,24,25,26,28,29,30,31, 32,34,37,38,39,41,44,51,55,57,61,63,64, 65,66,67,76,78 |
| Tidal flat facies | Mf4, Mf5 | 42,45,47,48 |
| Platform margin sand shoal facies | Mf2, Mf3 | 40,41,48,49,50,52,55,57,65,66,69,72,73, 74,75,78,79 |
| Inner shelf facies | Mf1 | 1,2,3,4,8,9,10,14,15,16,17,18,19,20,21, 30,33 |

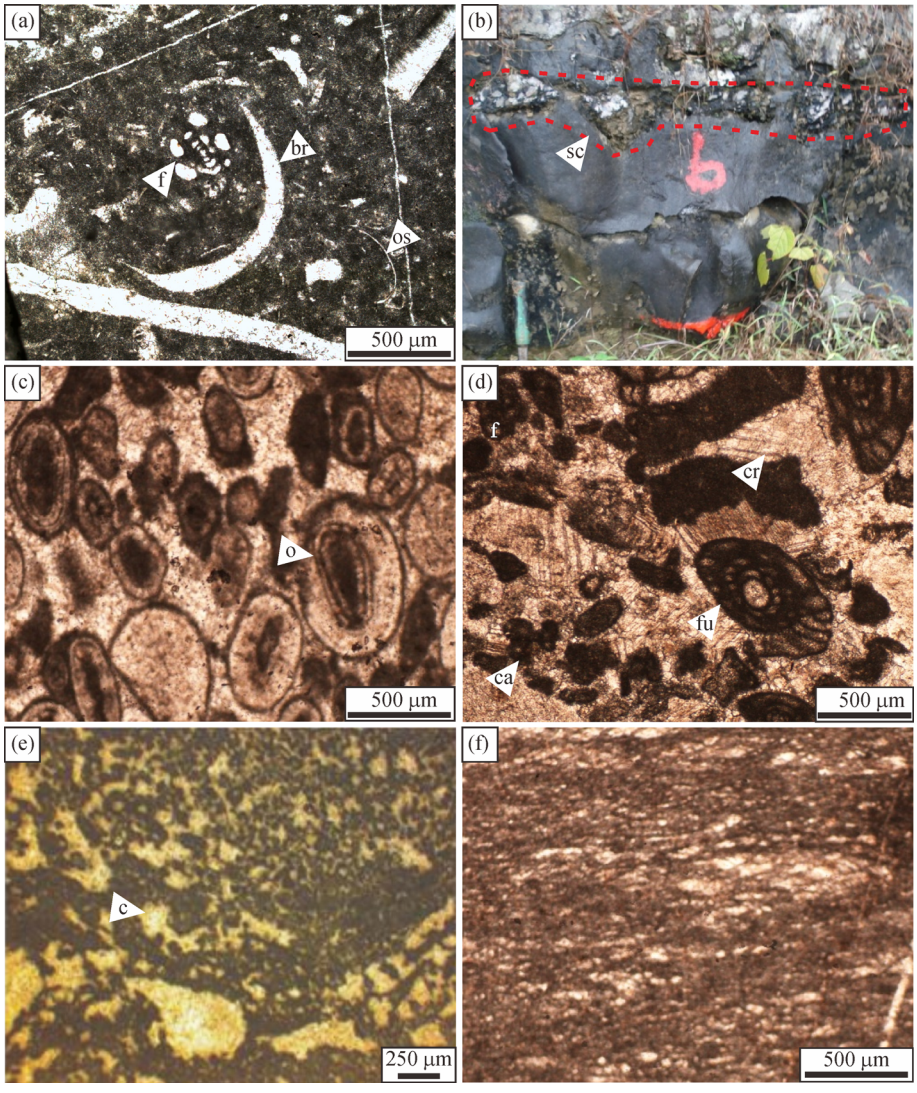


**Fig. 4** Typical microfacies types and Outcrop photograph from the Long'an section. (a) Lime mudstone (Mf1), bed 19, Long'an Formation; (b) Chert nodules (Mf1), bed 30, Long'an Formation; (c) Oolitic Grainstone (Mf2), bed 45, Du'an Formation; (d) Bioclastic grainstone (Mf3), bed 73, Huanglong Formation; (e) Fenestral boundstone (Mf4), bed 46, Du'an Formation; (f) Calcareous algal boundstone (Mf5), bed 47, Du'an Formation. Legend: br—brachiopods; c—cavities; f—foraminifera; o—oncoids; fu—fusulinids; cr —crinoids; ca—calcareous algae; sc—siliceous conglomerations; os-ostracods.

tidal flat facies above the platform margin shoals.

**Mf5: Algal boundstone**

Algal boundstone is mainly distributed in the Du'an Formation. Algal boundstone consists of algal filaments and algae laminae that are similar to the stromatolites (Fig. 4(d)). Other kind of fossils are seldom observed. This microfacies is interpreted as a high energy tidal flat facies above the platform margin shoals.

**Mf6: Bioclastic intraclast grainstone**

Bioclastic intraclast grainstone is mainly distributed in the Huanglong Formation, Maping Formation and mid-low part of the Du'an Formation. The grain content is more than 50%, and these grains include bioclast grains and intraclast grains (Fig. 5(a)). The intraclast grains normally formed in a high energy-shallow sea environment that was mainly influenced by wave forces. This observation indicates an open platform facies adjacent to platform margin sand shoals with moderate-high energy above the fair-weather wave base.

**Mf7: Bioclastic intraclast wackestone**

Bioclastic intraclast wackestone is mainly distributed in the Huanglong Formation, Maping Formation and the middle part of the Du'an Formation. The grain components are mainly intraclast grains (10%–25%), which are cemented by micrite calcite. Most of the intraclasts are argillaceous, and a few are foraminifera and echinoderm grains (Fig. 5(b)). This microfacies represents an open platform facies adjacent to platform margin sand shoals

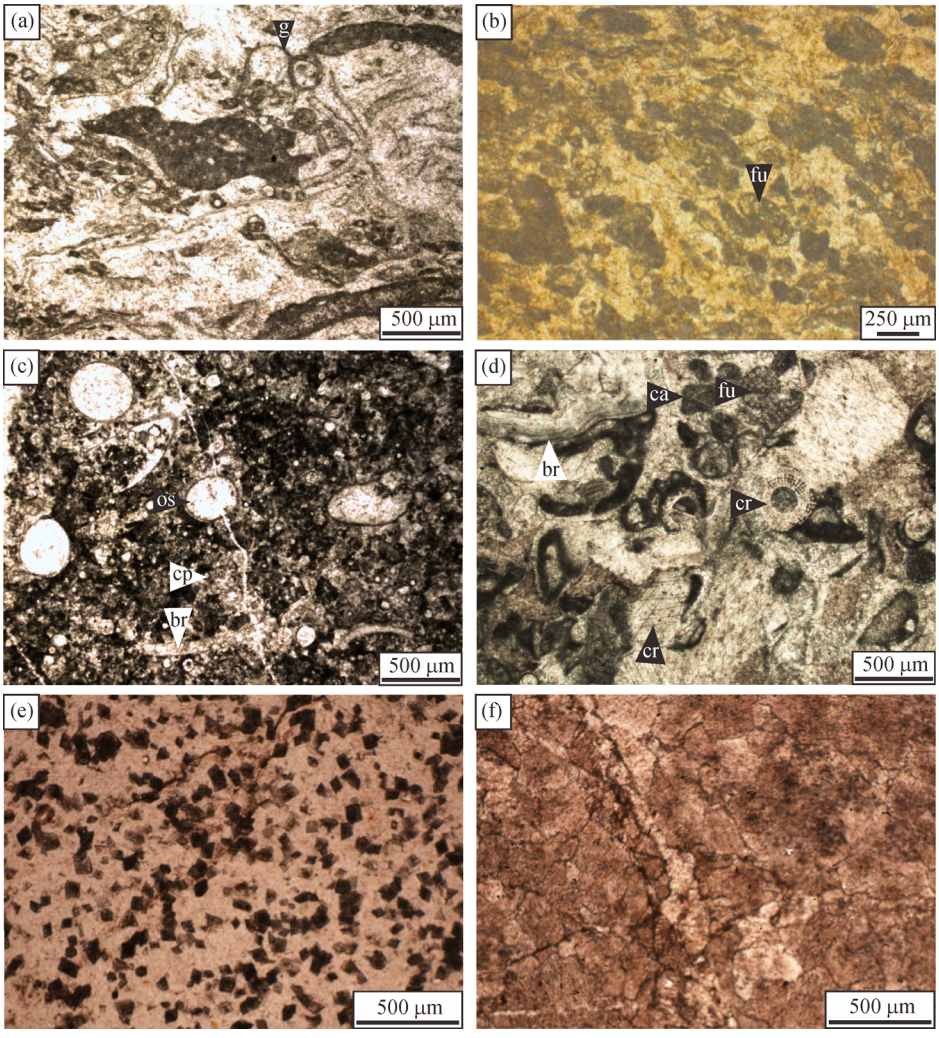


**Fig. 5** Typical microfacies types from the Long'an section. (a) Bioclastic intraclast grainstone (Mf6), bed 52, Du'an Formation; (b) Bioclastic intraclast wackestone (Mf7), bed 67, Huanglong Formation; (c) Bioclastic packstone (Mf8), bed 3, Rongxian Formation; (d) Bioclastic wackestone (Mf9), bed 70, Huanglong Formation; (e) Dolomite limestone (Mf10), bed 27, Long'an Formation; (f) Dolomite (Mf11), bed 52, Du'an Formation. Legend: g—gastropods; cp—calcispheres; br—brachiopods; fu—fusulinids; cr —crinoids; ca—calcareous algae; os-ostracods.

with low–moderate energy below the fair-weather wave base.

**Mf8: Bioclastic packstone**

Bioclastic packstone is usually distributed in the Huanglong Formation and Du'an Formation and in the upper part of the Long'an Formation. The grain types are mainly bioclasts including crinoids, brachiopods, calcareous algaes, foraminifera, fusulinids, etc. The fossils are well preserved and are cemented by micrite calcite (Fig. 5 (c)). This microfacies represents an open platform facies with low–moderate energy below the fair-weather wave base.

**Mf9: Bioclastic wackestone**

Bioclastic wackestone is usually distributed in the Long'an Formation. The matrix content is more than 50%, the grain components are mainly bioclasts including calcareous algae, crinoid stems, brachiopods, ostracods, etc. (Fig. 5(d)). This observation indicates an open platform environment or a restricted platform facies with low energy below the fair weather wave base.

**Mf10: Dolomite limestone**

Dolomite limestone is commonly distributed in middle part of the Long'an Formation. The dolomite content is between 25%–50%. The crystal forms change significantly from idiomorphic to hypidiomorphic with a low degree of dolomitization. Bioclasts are commonly cemented among the dolomite grains, and the matrix is sparry calcite (Fig. 5(e)). This observation indicates a restricted platform facies with low energy above the fair weather wave base.

**Mf11: Dolomite**

Dolomite is usually distributed in the Dapu Formation

and Huanglong Formation. This kind of fine-grained metasomatic dolomite with poor crystal form formed in different diagenetic environments. Dolomite generally piled up with hypidiomorphic and xenomorphic grains that are commonly 200–400 μm in size (Fig. 5(f)). This observation indicates a restricted platform facies with low energy above the fair weather wave base.

### 4.3 Carbon isotope stratigraphy of the Long'an section

The $\delta^{13}C$ values varied between −0.83‰ and 2.35‰ in the Famennian at the base of the Long'an section and showed multiple, brief positive $\delta^{13}C$ shifts. The $\delta^{13}C$ values varied between −0.67‰ and 2.61‰ in the *Siphonodella sinensis* zone, with two brief positive $\delta^{13}C$ shifts in the lower part of the *Siphonodella sinensis* zone. These two shifts had the amplitude of 2.30‰ and 2.39‰ respectively. The first major positive shift in $\delta^{13}C$ values, with an amplitude of 4.19‰, was measured in the *Siphonodella dasaibaensia* zone. The $\delta^{13}C$ values were relatively steady in the mid-late Toumaisian, with amplitudes of approximately 2.77‰. The $\delta^{13}C$ values sharply decreased in the *Polygnathus communis porcatus* zone, declining from 3.11‰ to −1.42‰, showing a pronounced negative excursion. After a small fluctuation, the $\delta^{13}C$ values then increased sharply from −2.04‰ to 3.23‰ in the late Visean. Following peak values of 3.32‰ in the latest Visean, the $\delta^{13}C$ values began to gradually decrease from 3.32‰ to −0.25‰ in the early to late Visean. The values then increased sharply by 2.82‰ across the Visean-Serpukhovian boundary. This sharp increase represented the second major positive shift. After a short stable phase, the $\delta^{13}C$ values decreased from 2.47‰ to 0.87‰, and then quickly rose to 2.82‰. The $\delta^{13}C$ values showed a negative shift during the middle Serpukhovian, and quickly decreased to −0.54‰. This negative shift may reflect the influence of slight meteoric diagenesis for the shallowest water facies in the Long'an section. Following a rapid increase to 2.38‰, the $\delta^{13}C$ values entered a stable phase and then increased from 1.30‰ to 2.40‰ in the Serpukhovian. This phenomenon represents the third major positive shift. Relatively steady $\delta^{13}C$ values of approximately 2.58‰ were seen in the early to middle Bashkirian. There were only small fluctuations in the uppermost part of the *Profusulinella-Pseudostaffella* zone. The $\delta^{13}C$ values began to decrease gradually, from 2.31‰ to −1.67‰, in the *Fusulinella-Fusuline* zone. The levels then abruptly increased to 0.35‰. After a short stable phase, there was a rapid increase to 1.26‰ and then an increase to a maximum level of 2.14‰ in the Kasimovian. The $\delta^{13}C$ values demonstrated a continuous step-wise increase that shows a fourth clear positive excursion with an amplitude of 3.69‰. The $\delta^{13}C$ values in the *Pseudoschwagerina* zone are slightly higher than in the *Triticites* zone (Fig. 6).

## 5 Discussion

### 5.1 Validity Analyses of Carbon isotopes in Carbonate Rocks

Valid sample data are essential to the study of the carbon stable isotopic stratigraphy. As such, to ensure the validity of the carbon and oxygen stable isotopic data, we first considered the related sedimentary environments and diagenesis. Here, we offer three identifying criteria to indicate whether the carbon and oxygen isotopes in the carbonate rocks experienced alterations during diagenesis.

1) $\delta^{18}O$ distinguishing method. Evidence from previous studies has confirmed that when $\delta^{18}O < -5‰$, oxygen isotopes vary significantly. When $\delta^{18}O < -10‰$, the oxygen isotopes change significantly, and the related carbon isotope data are invalid (Kaufman and Knoll, 1995). The $\delta^{18}O$ values in the Long'an section ranged from −8.87‰ to −0.43‰. A majority of the samples are characterized by $\delta^{18}O > -5‰$; this result indicates little resetting of carbon isotope levels by meteoric diagenesis.

2) $\delta^{13}C$ and $\delta^{18}O$ correlation method. If the $\delta^{13}C$ and $\delta^{18}O$ values are positively correlated, the carbonate rocks are recognized as being influenced by meteoric diagenesis during diagenesis. The $\delta^{13}C$ and $\delta^{18}O$ values suggest that the Carboniferous carbonate rocks in the Long'an section were not significantly influenced by the meteoric diagenesis during diagenesis (Fig. 7).

3) The Mn/Sr ratio is often used in the analysis of diagenesis because Mn is more likely to enter carbonate minerals during diagenesis, while Sr is more likely to be released from carbonate minerals. As a result, the Mn/Sr ratios are obviously higher in samples affected by diagenesis. Kaufman and Knoll (1995) believed that when the Mn/Sr ratio is less than 10, the $\delta^{13}C_{carb}$ basically retained the carbon isotope composition characteristics of the original ocean. The Mn/Sr ratios of the samples studied here are all below 2.0, far lower than the threshold value identified above for diagenesis.

The carbon and oxygen isotopes from the Long'an section fall mainly within or near updip/downdip Fe-calcite cement fields, indicating a weak influence from burial diagenesis. The $\delta^{13}C$ values fall within a burial regime, which was effectively a closed system with respect to carbon (Hudson, 1975; Qie et al., 2014). Only three samples lie within or near the early meteoric calcite cement field (CLA-W2-1,CLA-I-11-b,CLA-I-34-a), reflecting the influence of meteoric diagenesis, and the $\delta^{18}O$ values of the three samples with $\delta^{18}O$ values $> -10‰$ indicates no significant influence by meteoric diagenesis.

### 5.2 Carbon isotope events

The variations in carbon isotope values across geologic time indirectly reflect the variations in global carbon

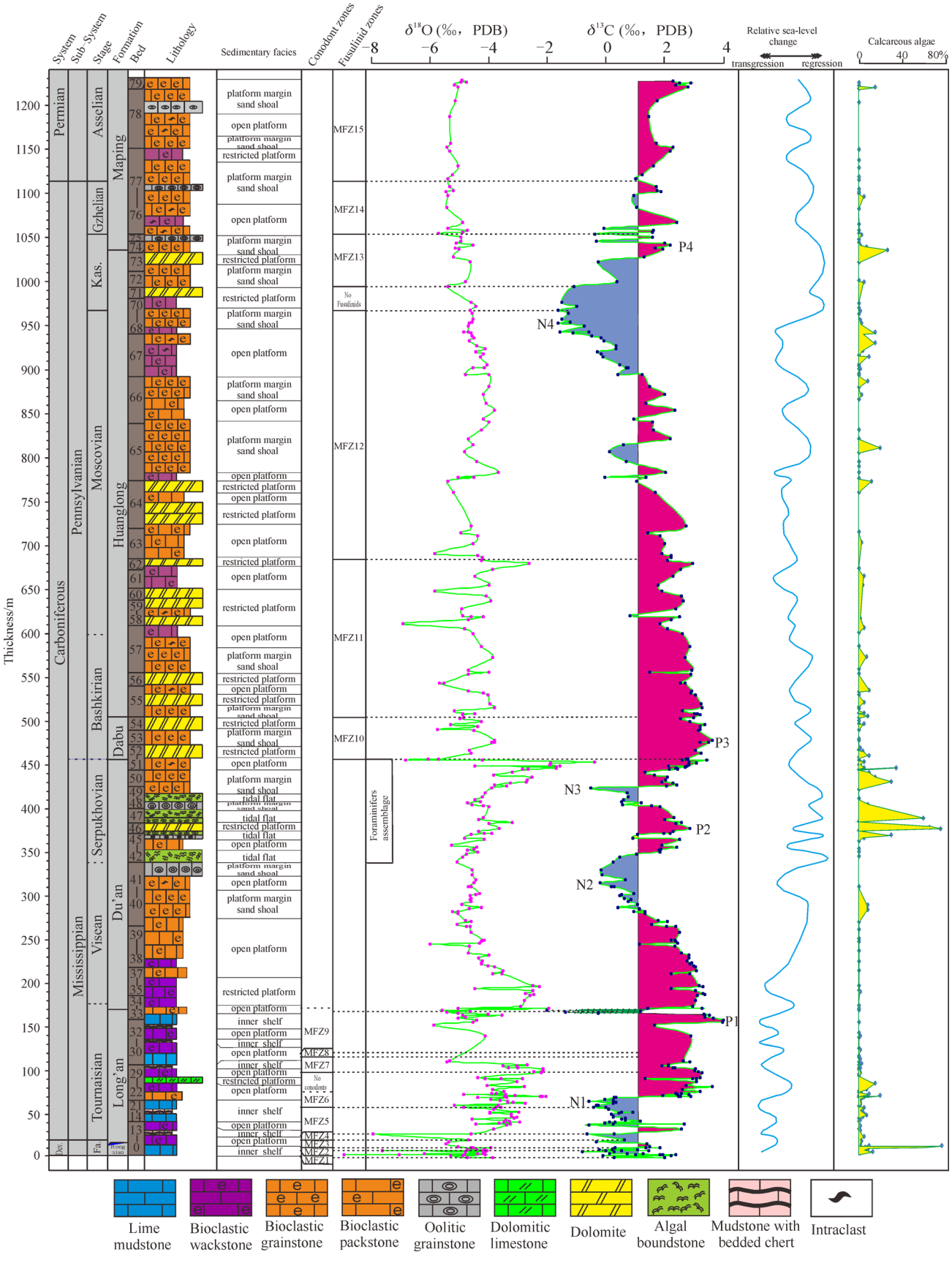


**Fig. 6** A comprehensive graph showing the lithological columnar chart of the Long'an section biozones and $\delta^{13}C$ and $\delta^{18}O$ variation curves. Among these biozones, the conodont zones were identified based on Qie et al., (2010, 2014, and 2015). These are shown in the graph as MFZ1 = Lower *Siphonodella praesulcata* zone; MFZ2 = Middle *Siphonodella praesulcata* zone; MFZ3 = Upper *Siphonodella praesulcata* zone; MFZ4 = *Siphonodella homosimplex* zone; MFZ5 = *Siphonodella sinensis* zone; MFZ6 = *Siphonodella dasaibaensis* zone; MFZ7 = *Polygnathus communis carina* zone; MFZ8 = *Gnathodus cuneiformis* zone; and MFZ9 = *Polygnathus communis porcatus* zone. The fusulinid biozones: MFZ10 = *Pseudostaffella* zone; MFZ11 = *Profusulinella* zone; MFZ12 = *Fusulina-Fusulinella* zone; MFZ13 = *Triticites* zone; MFZ14 = *Quasifusulina* zone; and MFZ15 = *Pseudoschwagerina* zone. LM-Lime mudstone. (blue areas represents negative shifts, pink areas represent for positive shifts)

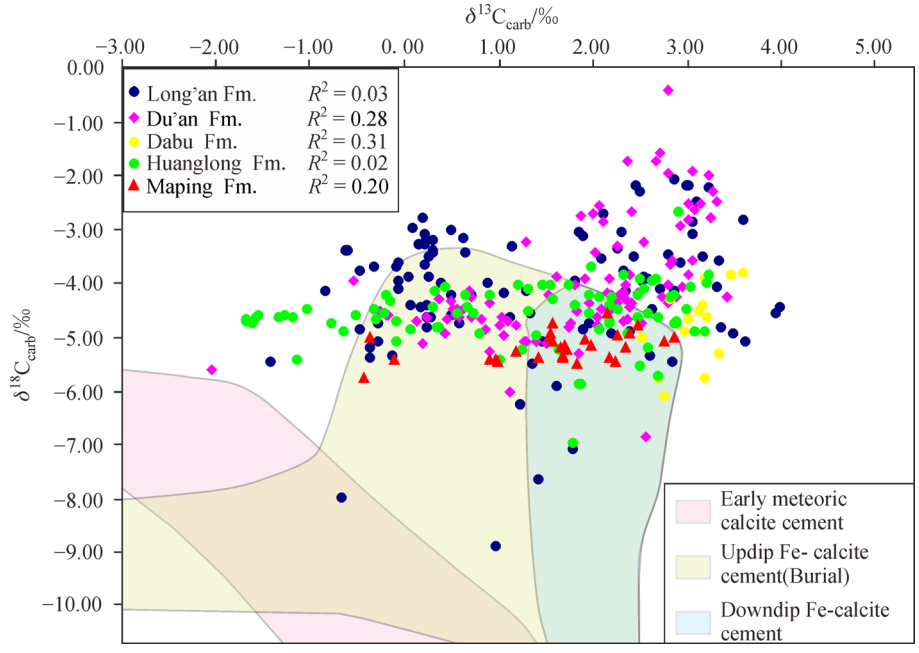


**Fig. 7** $\delta^{13}C$ and $\delta^{18}O$ crossplots from different formations in the Long'an section (Wynn and Read, 2007).

cycling. Significant shifts are consistently correlated with significant paleoclimatic and paleoenvironmental events, which greatly influenced biological evolutionary processes (Peng et al., 2016). A positive shift of carbon isotope values relates to the burial of abundant organic carbon (Bruckschen et al., 1999; Saltzman, 2003), the cooling of the climate (Mii et al., 2001), and the promotion of primary productive capacity (Buggisch et al., 2008). However, negative excursions typically indicate massive biological extinctions (Magaritz et al., 1986), methane releases (Jiang et al., 2003; Wang et al., 2008), and volcanic eruptions (Shen et al., 2012).

The Late Paleozoic Ice Age was one of the most important paleoclimate transitions in earth's geological history. Isbell et al. (2003) defined three glaciation time intervals: Glacial I, Glacial II, and Glacial III. These three glacial intervals in the late Paleozoic correlate with positive $\delta^{13}C$ shifts (Mii et al., 1999 and 2001; Saltzman et al., 2000 and 2003; Buggisch et al., 2008; Grossman et al., 2008). Meanwhile, the Late Ordovician ice age was perfectly correlated with the observed carbon isotope values (Marshall et al., 1997; Saltzman and Young, 2005; Liu et al., 2016). We can couple the global $\delta^{13}C$ positive excursions with the global sea-level falls as one of the criteria to identify the ice age in the Late Paleozoic.

### 5.2.1 Brief $\delta^{13}C$ positive shifts

The $\delta^{13}C$ levels showed five brief positive shifts at the base of the Long'an section during the late Famennian and two brief positive $\delta^{13}C$ shifts in the lower part of the *Siphonodella sinensis* zone in the early Tournaisian. These multiple brief positive $\delta^{13}C$ shifts, accompanied by positive $\delta^{18}O$ shifts, reflect cooling events that occurred during the late Famennian to early Tournaisian (Fig. 6). In the meantime, the glacial deposits in the Brazilian Amazon basin and in the Paranaiba Basin during the late Famennian to early Tournaisian mark the start of the late Paleozoic ice age (Caputo, 1985; Streel et al., 2000; Isaacson et al., 2008). The glaciation is considered to have been alpine (Isbell et al., 2003) and to have coincided with Glacial I (Isbell et al., 2003). In addition, the $\delta^{13}C$ positive shift in the Middle *Siphonodella praesulcata* zone reflects the Hangenberg Event (Qie et al., 2015).

### 5.2.2 The first major $\delta^{13}C$ positive shift

In the Long'an section, the first major positive shift of $\delta^{13}C$ with an amplitude of 4.19‰, occurred in the *Siphonodella dasaibaensia* zone of the Tournaisian (Qie et al., 2010). This positive shift also occurred in Europe, the US Midcontinent, and the Russian Platform. In Europe and North America, the $\delta^{13}C$ shift was greater than 3.0‰ (Buggisch et al., 2008); in the Moscow basin, the shift was greater than 4.0‰ (Bruckschen et al., 1999); and in the Arrow Canyon section in Nevada, US, the shift reached 7.0‰ (Fig. 8). This positive shift in $\delta^{13}C$ has been recognized as one of the most important carbon isotope events in the Phanerozoic (Saltzman et al., 2000). Saltzman et al. (2000 and 2003), Grossman et al. (2008), and Buggisch et al. (2008) have all proposed that this positive shift related to a massive burial of organic carbon, a

decrease in $pCO_2$, and global climate cooling. Furthermore, Buggisch et al. (2008) studied the $\delta^{18}O$ values in the conodonts in Europe-America and confirmed that this $\delta^{13}C$ positive shift was accompanied by an increase in $\delta^{18}O$ values, and these values also indicate glacial events and climate cooling. In terms of primary productivity, the average percentage of calcareous algae as the main primary producers in each layer of bioclastic statistics is significantly greater after the positive shift in $\delta^{13}C$ than before. This process showed an increase of primary productivity and that may have been the reason of the $\delta^{13}C$ positive shift.

From a sedimentology perspective, the lithology that emerged before the positive shift in $\delta^{13}C$ was a dark-gray thin-bedded lime mudstone (Fig. 4(a)), indicating an inner shelf environment. After the positive $\delta^{13}C$ shift, the lithology rapidly transitioned to dark-gray middle-bedded bioclastic packstone and bioclastic wackestone. This phenomenon indicates an open platform environment. Compared with the inner shelf environment, the open platform environment is more conducive to biological reproduction and also provides conditions for the burial of organic carbon.

This positive shift in $\delta^{13}C$ is also accompanied by a sea-level drop in the Long'an area. Studies have also revealed sea-level decrease events not only in other places in South China (Li et al., 1997) but also in North America. The upper Kinderhookian-Osagean Lodgepole Formation is a dominantly carbonate succession. This succession contains juxtaposed facies, which are interpreted as recording 20–25 m glacioeustatic fluctuations (Elrick and Read, 1991). In Ohio, the Black Hand Sandstone has been reinterpreted as a paleovalley, formed in response to a 60 m sea-level drop during the development of the Kinderhookian-Osagean unconformity in North America (Matchen and Kammer, 2006). In conclusion, this $\delta^{13}C$ positive shift that was synchronized with the sea-level fall has global correlations. Temporally, this shift coincided with the Glacial I (Isbell et al., 2003).

### 5.2.3 The second major $\delta^{13}C$ positive shift

In the Visean-Serpukhovian, the $\delta^{13}C$ values show similar evolutionary trends in South China, the US Midcontinent, and the Russian Platform (Bruckschen et al., 1999; Buggisch et al., 2011) (Fig. 8). In the early Visean, $\delta^{13}C$ showed relatively higher positive values; in the middle to late Visean, however, the $\delta^{13}C$ values gradually shifted lower, which presented a trend of a negative shift. From the late Visean to early Serpukhovian, the $\delta^{13}C$ values rapidly increased again to 2.38‰. This rapid increase marks the second major positive shift during the Carboniferous. This obvious positive shift in $\delta^{13}C$ was also reported in western Europe and in the Moscow Basin (Bruckschen et al., 1999). It is worth noting that, after the $\delta^{13}C$ positive shift, the content of calcareous algae increased rapidly from a very low value to a peak value, which indicated that the $\delta^{13}C$ positive shift may have been triggered by an increase in primary productivity.

Consistent with the positive shift of $\delta^{13}C$, the early Serpukhovian showed an obvious sea-level drop in the Long'an section. The lithology that emerged before the positive shift in $\delta^{13}C$ was bioclastic intraclast grainstone and bioclastic packstone, indicating an open platform environment. After the positive $\delta^{13}C$ shift, the lithology rapidly transitioned to oolitic grainstone (Fig. 3(c)), algal boundstone (Fig. 4(f)) and fenestral boundstone (Fig. 4(e)). This phenomenon indicates a platform margin sand shoal or tidal flat environment. In the Nandan, Guangxi Province, a sea-level regression event occurred in this period (Qie et al., 2010). This sea-level drop is also recognized in the Luodian and Huishui in Guizhou Province (Chen et al., 2016). In North America, the presence of paleoweathered crusts in the Illinois Basin and in the Precordilleran Mountains reflect glacioeustatic fluctuations (González-Bonorino, 1992; Smith and Read, 2000).

### 5.2.4 The third major $\delta^{13}C$ positive shift

In the early Serpukhovian, $\delta^{13}C$ showed relatively higher positive values, in the early-mid Serpukhovian, the $\delta^{13}C$ values shifted negatively to –0.54‰. In the middle Serpukhovian, the $\delta^{13}C$ values experienced a continuous step-wise increase from –0.54‰ to 2.38‰. After a short stabilization period, the values started at 1.30‰ and increased to 2.40‰ (Fig. 6). This increase in $\delta^{13}C$ values represents the third positive shift in the Carboniferous. According to the statistical analysis of the percentage of bioclasts in thin sections, the contents of calcareous algae were at very low levels before the occurrence of the $\delta^{13}C$ positive shift but rapidly increased after that. This process indicated an improvement in primary productivity. Globally, in south-western Nevada, in the US Midcontinent, and in the Russian Platform (Bruckschen et al., 1999; Saltzman, 2003; Grossman et al., 2008) (Fig. 8), the shifts in $\delta^{13}C$ values during this period were all positive. Meanwhile, $\delta^{18}O$ dropped to its lowest values in the middle Serpukhovian and further increased rapidly in the late Serpukhovian (Saltzman, 2003; Grossman et al., 2008). Consistent with the positive shifts of $\delta^{13}C$ and $\delta^{18}O$, most European-American areas experienced the largest sea-level regression in this period (Ross and Ross, 1988). The correlated sediments in the upper Du'an Formation and Dapu Formation consist mainly of bioclastic grainstone and dolomite (Fig. 5(f)). These composition indicate a carbonate platform shoal or restricted platform environment. In addition, Gondwana experienced widespread deposition of glacial sediments (Garzanti and Sciunnach, 1997; Isbell et al., 2003). All of this evidence indicates that

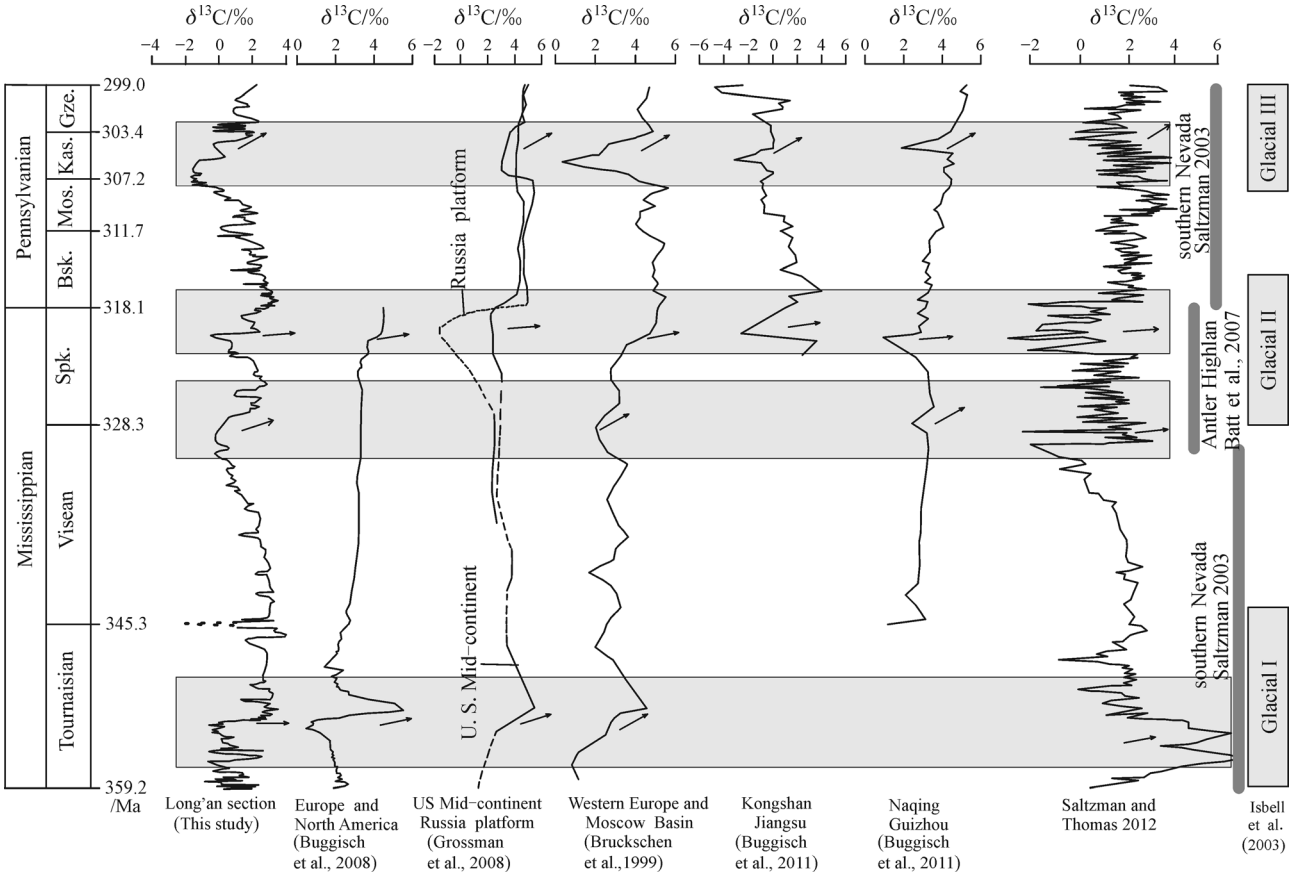


**Fig. 8** A comprehensive graph showing the contrasts in the evolution of carbon isotope values among the Carboniferous system carbonates in the Long'an section in South China, the carbonates in Europe and North America (Buggisch et al., 2008), the mean values of carbon isotope values from calcite in brachiopod shells on the Russian platform and the US Mid-continent (Grossman et al., 2008), the carbon isotope values from calcite in brachiopod shells in western Europe and Moscow Basin (Bruckschen et al., 1999), the Kongshan area in Jiangsu, and the Naqing area of Guizhou (Buggisch et al., 2008), and the southern Nevada and Antler Highland (Saltzman and Thomas, 2012). The absolute age values are based on Cohen et al. (2013).

the major $\delta^{13}C$ positive shift marked the start of widespread glaciation. Temporally, this positive shift coincided with the Glacial II (Isbell et al., 2003).

### 5.2.5 The fourth major $\delta^{13}C$ positive shift

In the Long'an section, the $\delta^{13}C$ values showed a gradual decline throughout the Moscovian, reaching their lowest values of −1.67‰ at the top of the *Fusulinella–Fusulina* zone. After crossing the Moscovian/Kasimovian boundary, the $\delta^{13}C$ values immediately increased from −1.55‰ to 0.35‰. After a short stabilization period, these values increased rapidly from −0.30‰ to 1.26‰, reaching a maximum of 2.14‰ at the top of the *Triticites* zone in the Kasimovian. These variations represented the fourth obvious $\delta^{13}C$ positive excursion.

Similar variations were seen in Europe, the US Mid-continent, western North America, and the Russian Platform (Fig. 8). In the Russian Platform, $\delta^{13}C$ values steadily fluctuated within relatively higher ranges in the Bashkirian and early Moscovian. In the late Moscovian, however, the $\delta^{13}C$ values began to drop, reaching their lowest values in the early Kasimovian. The values then began to increase, until reaching a maximum in the early Gzhelian (Grossman et al., 2008). In the Guadalupe Mountains area of the US Midcontinent, the $\delta^{13}C$ values decreased in the late Moscovian; the lowest values were concentrated in the early Kasimovian. Soon after, the values began to rise, reaching a maximum in the Gzhelian (Grossman et al., 2008). In South China, the Zongdi, Kongshan, and Naqing sections all showed similar evolutionary tendencies (Buggisch et al., 2011). All of the above evidence shows that the $\delta^{13}C$ positive excursion in this area was globally significant. Moreover, studies of the $\delta^{18}O$ values in brachiopod shells from the Russian Platform confirmed the $\delta^{18}O$ positive shift from the Kasimovian to the Asselian. These values also act as indicators of ice age events and are correlated with climate cooling (Grossman et al., 2008).

In the late Moscovian, a clear sea-level drop is seen in

the Long'an section, coinciding with the negative $\delta^{13}C$ spike. The sediments of the upper Huanglong Formation were deposited with bioclastic grainstone (Fig. 4(d)), dolomitic limestone and dolomite, indicating a bioclastic shoal or restricted platform environment. The sea-level drop is also recognized in the deep-water Dian-Qian-Gui Basin (Li et al., 1997; Mei and Li, 2004; Mei et al., 2005) and in Hunan Province (Huang et al., 2017), which contains dolomitic and grainstone textures. Rygel et al. (2008) also reported a synchronous sea-level drop of 100–120 m in South America. In the late Pennsylvanian, a large sea-level decline was seen in the Oklahoma area. From the late Carboniferous to early Permian, glacial sediments were widely distributed in Australia, Africa, the Arabian Peninsula, Madagascar, India, and South America (Veever and Powell, 1987; Isbell et al., 2003; López-Gamundí and Bauatois, 2010). The relatively low sea level in the Long'an area during the Kasimovian, correlated with $\delta^{13}C$ positive shift, is attributed to the growth of the Gondwanan ice sheet (Liu et al., 1994; Li et al., 1996). Temporally, this $\delta^{13}C$ positive shift coincided with the Glacial III (Isbell et al., 2003).

It worth noting that the $\delta^{13}C$ values associated with the positive shifts in South China are consistent with those in other places in the world. The peak values and amplitudes differ from place to place; this variation may be due to different organic carbon burial volumes and velocities in different paleoenvironments and to different weathering intensities (Grossman et al., 2008).

## 6 Conclusions

1) Foraminiferal assemblages in the upper Du'an Formation indicate a Serpukhovian age. Six fusulinid genozones, namely, (in ascending order) the *Pseudostaffella* zone, *Profusulinella* zone, *Fusulinella-Fusulina* zone, *Triticites* zone, *Quasifusulina* zone and *Pseudoschwagerina* zone, can be recognized in the Bashkirian to Asselian successions in the Long'an area.

2) Four obvious $\delta^{13}C$ positive shifts were identified in the Long'an section during the Carboniferous. The first obvious positive shift with an amplitude of 4.19‰ occurred in the middle of the Tournaisian. This shift corresponds to the *Siphonodella dasaibaensia* zone and reflects massive burial of organic carbon and a global cooling event. The second obvious positive shift occurred around the boundary of the Visean/Serpukhovian with an amplitude of 2.63‰ and is regarded as being related to a glacioeustatic marine regression. The third obvious positive excursion with an amplitude of 3.95‰ occurred in the middle Serpukhovian and is correlated to the regression event and to globally widespread glacial sediments. The fourth obvious positive excursion with an amplitude of 3.69‰ occurred in the Kasimovian. This shift is correlated with the glacioeustatic marine regression in the European-American areas and in South China, the massive burial of organic carbon, and with globally widespread glacial sediments. Furthermore, there were several brief positive $\delta^{13}C$ shifts during the late Famennian to early Tournaisian in the Long'an section, and these shifts coincide well with glacial sediments in South America. The positive $\delta^{13}C$ shift in the middle *Siphonodella praesulcata* zone reflects the Hangenberg Event.

3) The four significantly positive $\delta^{13}C$ shifts in the Carboniferous in the Long'an section correspond well to the European-American areas from a temporal perspective. The four major positive $\delta^{13}C$ shifts combined with several brief positive $\delta^{13}C$ shifts during the late Famennian to early Tournaisian correspond to the well-accepted Glacial I, II, and III events. The carbon isotope data reflect an increase in primary productivity and global climate cooling. These data have also revealed the carbon isotope responses of the Gondwanan ice age in South China.

**Acknowledgements** This paper has received both technical and financial supports respectively from the National Basic Research Program of China under the State Key Laboratory of Geological Process and Mineral Resources, China University of Geosciences (Wuhan) (No. KZ11K312), the National Natural Science Foundation of China (Grant No. 41702366) and the Fundamental Research Funds for the Central Universities (No. 3142018004)

## References

Bruckschen P, Oesmann S, Veizer J (1999). Isotope stratigraphy of the European Carboniferous: proxy signals for ocean chemistry, climate and tectonics. Chem Geol, 161(1–3): 127–163

Buggisch W, Joachimski M M, Sevastopulo G, Morrow J R (2008). Mississippian $\delta^{13}C$ carb and conodont apatite $\delta^{18}O$ records—their relation to the Late Palaeozoic Glaciation. Palaeogeogr Palaeoclimatol Palaeoecol, 268(3–4): 273–292

Buggisch W, Wang X D, Alekseev A S, Joachimski M M (2011). Carboniferous–Permian carbon isotope stratigraphy of successions from China (Yangtze platform), USA (Kansas) and Russia (Moscow Basin and Urals). Palaeogeogr Palaeoclimatol Palaeoecol, 301(1–4): 18–38

Caputo M V (1985). Late Devonian glaciation in South America. Palaeogeogr Palaeoclimatol Palaeoecol, 51(1–4): 291–317

Caputo M V, Crowell J C (1985). Migration of glacial centers across Gondwana during Paleozoic Era. Geol Soc Am Bull, 96(8): 1020–1036

Chen J T, Montañez I P, Qi Y P, Wang X D, Wang Q L, Lin W (2016). Coupled sedimentary and $\delta^{13}C$ records of late Mississippian platform-to-slope successions from South China: insight into $\delta^{13}C$ chemostratigraphy. Palaeogeogr Palaeoclimatol Palaeoecol, 448: 162–178

Cohen K M, Finney S C, Gibbard P L (2013). The ISC international chronostratigraphic chart. Episodes, 36: 199–204

Crowell J C (1978). Gondwana glaciation, cyclothems, continental positioning and climate change. Am J Sci, 278(10): 1345–1372

Elrick M E, Read J F (1991). Cyclic ramp-to-basin carbonate deposits,

Lower Mississippian, Wyoming, and Montana. J Sediment Petrol, 61: 1194–1224

Feng Z Z, Yang Y Q, Bao Z D (1998). Lithofacies Palaeogeography of the Carboiferous in South China. Beijing: Geological Publishing House

Flügel E (2010). Microfacies of Carbonate Rocks: Analisis, Interpretation and application. Berlin, Heidelberg: Springer-Verlag

Frakes L A, Francis J E, Syktus J I (1992). Climate Modes of the Phanerozoic. London: Cambridge University Press

Garzanti E, Sciunnach D (1997). Early Carboniferous onset of Gondwanian glaciation and Neo-tethyan rifting in South Tibet. Earth Planet Sci Lett, 148(1–2): 359–365

González-Bonorino G (1992). Carboniferous glaciation in Gondwana: evidence for grounded marine ice and continental glaciation in southwestern Argentina. Palaeogeogr Palaeoclimatol Palaeoecol, 91 (3–4): 363–375

Grossman E L, Yancey T E, Jones T E, Bruckschen P, Chuvashov B, Mazzullo S J, Mii H (2008). Glaciation, aridification, and carbon sequestration in the Permo-Carboniferous: the isotopic record from low latitudes. Palaeogeogr Palaeoclimatol Palaeoecol, 268(3–4): 222–233

Huang X, Aretz M, Zhang X H, Du Y S, Qie W K, Wen Q, Wang C N, Luan T F (2017). Pennsylvanian-early Permian palaeokarst development on the Yangtze Platform, South China, and implications for the regional sea-level history. Geol J, 53(4): 1241–1262

Hudson J D (1975). Carbon isotopes and limestone cement. Geology, 3 (1): 19–22

Isaacson P E, Díaz-Martínez E, Grader G W, Kalvoda J, Babek O, Devuyst F X (2008). Late Devonian-earliest Mississippian glaciation in Gondwanaland and its biogeographic consequences. Palaeogeogr Palaeoclimatol Palaeoecol, 268(3–4): 126–142

Isbell J L, Miller M F, Wolfe K L, Lenaker P A (2003). Timing of late Paleozoic glaciation in Gondwana: was glaciation responsible for the development of Northern hemisphere cyclothems? Spec Pap Geol Soc Am, 370: 5–24

Jiang G, Kennedy M J, Christie-Blick N (2003). Stable isotopic evidence for methane seeps in Neoproterozoic postglacial cap carbonates. Nature, 426(6968): 822–826

Kabanov P B, Alekseev A S, Gibshman N B, Gabdullin R R, Bershov A V (2016). The upper Viséan–Serpukhovian in the type area for the serpukhovian stage (Moscow Basin, Russia): part 1. sequences, disconformities, and biostratigraphic summary. Geol J, 51(2): 163–194

Kaufman A J, Knoll A H (1995). Neoproterozoic variations in the C-isotopic composition of seawater: stratigraphic and biogeochemical implications. Precambrian Res, 73(1–4): 27–49

Kuang G D, Li J J, Zhong J, Su Y B, Tao Y B (1999). The Carboniferous in Guangxi. Wuhan: China University of Geosciences Press

Li J C, Kuang D Z, Zhang Z H, Hong Z Y (2011). Late Carboniferous–early Permian fusulinid biostratigraphy of Shunchang, Fujian province. Acta Micropalaeontologica Sin, 28(3): 309–315

Li R F, Liu B P, Zhao C L (1996). Characteristics of cycle-sequence, carbon isotope features and glacio-eustasy of the Triticites zone in southern Guizhou. Acta Sedimentologica Sinica, 70(4): 342–350

Li R F, Liu B P, Zhao C L (1997). Correlation of Carboniferous depositional sequences on the Yangtze plate with other on a global scale. Acta Sedimentologica Sinica, 15(3): 23–28

Liu B P, Li R F, You D H (1994). Carboniferous sequence stratigraphy and glacio-eustasy of Triticites zone in southern Guizhou, China. Earth Sci J China U, 19: 553–564

Liu C G, Li G R, Wang D W, Liu Y L, Luo M X, Shao X M (2016). Middle–Upper Ordovician (Darriwilian–Early Katian) positive carbon isotope excursions in the northern Tarim Basin, Northwest China: implications for stratigraphic correlation and paleoclimate. J Earth Sci, 27(2): 317–328

Liu C, Jarochowska E, Du Y S, Vachard D, Munnecke A (2017). Stratigraphical and $\delta^{13}C$ records of Permo-Carboniferous platform carbonates, South China: responses to late Paleozoic icehouse climate and icehouse-greenhouse transition. Palaeogeogr Palaeoclimatol Palaeoecol, 474: 113–129

Lin C M, Ling H F, Wang S J, Zhang S (2002). Evolution regularities of carbon and oxygen isotopes in Carboniferous marina carbonate rocks from Jiangsu and Anhui provinces. Geochimica, 31(5): 415–423

López-Gamundí O R, Buatois L A (2010). Introduction: Late Paleozoic glacial events and postglacial transgressions in Gondwana. Geol Soc Am Bull, 468: 5–8

Magaritz M, Holser W T, Kirschvink J L (1986). Carbon-isotope events across the Precambrian/Cambrian boundary on the Siberian Platform. Nature, 320(6059): 258–259

Marshall J D, Brenchley P J, Mason P, Wolff G A, Astini R A, Hints L, Meidla T (1997). Global carbon isotopic events associated with mass extinction and glaciation in the late Ordovician. Palaeogeogr Palaeoclimatol Palaeoecol, 132(1–4): 195–210

Matchen D L, Kammer T W (2006). Incised valley fill interpretation for Mississippian Black Hand Sandstone, Appalachian Basin, USA: implications for glacial eustasy at Kinderhookian-Osagean (Tn2-Tn3) boundary. Sediment Geol, 191(1–2): 89–113

Ma Z L, Wang Y, Wang Q L, Hoshiki Y, Uene K, Qi Y P, Wang X D (2013). Biostratigraphy of the Bashlirian-Moscovian boundary interval at Luokun section in Guizhou, South China. Acta Palaeontologica Sinic, 52(4): 492–502

Mei M X, Li Z Y (2004). Sequence-stratigraphic succession and sedimentary-basin evolution from late Paleozoic to Triassic in the Yunnan-Guizhou-Guangxi region. Geoscience, 18: 555–563

Mei M X, Ma Y S, Deng J, Chu H M, Liu Z R, Zhang H (2005). Carboniferous to Permian sequence stratigraphic framework of the Yunnan-Guizhou-Guangxi basin and its adjacent areas and global correlation of third-order sea-level change. Geology in China, 32: 13–24

Mii H S, Grossman E L, Yancey T E (1999). Carboniferous isotope stratigraphies of North America: implications for Carboniferous paleoceanography and Mississippian glaciation. Geol Soc Am Bull, 111(7): 960–973

Mii H S, Grossman E L, Yancey T E, Chuvashov B, Egorov A (2001). Isotopic records of brachiopod shells from the Russian Platform-evidence for the onset of mid-Carboniferous glaciation. Chem Geol, 175(1–2): 133–147

Okuyucu C (2013). Fusulinid zonation of the Late Moscovian-Early Sakmarian sequences from the Taurides, southern Turkey. Neues Jahrb Geol Palaontol Abh, 268(3): 237–258

Peng Y, Peng Y B, Lang X G, Ma H, Huang K, Li F, Shen B (2016). Marine carbon-sulfur biogeochemical cycles during the steptoean

Positive Carbon Isotope Excursion (SPICE) in the Jiangnan basin, South China. J Earth Sci, 27(2): 242–254

Qie W K, Liu J S, Chen J T, Wang X, Mii H, Zhang X, Huang X, Yao L, Algeo T J, Luo G (2015). Local overprints on the global carbonate $\delta^{13}C$ signal in Devonian–Carboniferous boundary successions of South China. Palaeogeogr Palaeoclimatol Palaeoecol, 418: 290–303

Qie W K, Zhang X H, Cai X F, Zhang Y (2007). Geobiological processes and the formation of hydrocarbon source rocks in the Carboniferous-Early Permian glacial period in South China. Earth Sci J China U, 32(6): 803–810

Qie W K, Zhang X H, Du Y S, Zhang Y (2010). Lower Carboniferous carbon isotope stratigraphy in South China: implications for the Late Paleozoic glaciation. Sci China Earth Sci, 40(11): 1533–1542

Qie W K, Zhang X H, Du Y S, Yang B, Ji W T, Luo G M (2014). Conodont biostratigraphy of Tournaisian shallow-water carbonates in central Guangxi, South China. Geobios, 47(6): 389–401

Ross C A, Ross J R P (1988). Late Paleozoic transgressive-regressive deposition. SEPM Special Publication, 42: 227–247

Rygel M C, Fielding C R, Frank T D, Birgenheier L P (2008). The magnitude of Late Paleozoic glacioeustatic fluctuations: a synthesis. J Sediment Res, 78(8): 500–511

Saltzman M R, González L A, Lohmann K C (2000). Earliest Carboniferous cooling step triggered by the Antler orogeny? Geology, 28(4): 347–350

Saltzman M R (2002). Carbon and oxygen isotope stratigraphy of the Lower Mississippian (Kinderhookian–lower Osagean), western United States: implications for seawater chemistry and glaciation. Geol Soc Am Bull, 114(1):96–108

Saltzman M R (2003). Late Paleozoic ice age: oceanic gateway or $pCO_2$? Geology, 31(2): 151–154

Saltzman M R, Thomas E (2012). Carbon isotope stratigraphy. In: Gradstein F, Ogg J, Schmitz M, Ogg G, eds. The Geologic Time Scale 2012. Boston: Elsevier, 221–246

Saltzman M R, Young S A (2005). Long-lived glaciation in the Late Ordovician? Isotopic and sequence-stratigraphic evidence from western Laurentia. Geology, 33(2): 109–112

Shen J, Algeo T J, Hu Q, Zhang N, Zhou L, Xia W C, Xie S C, Feng Q L (2012). Negative C isotope excursions at the Permian-Triassic boundary linked to volcanism. Geology, 40(11): 963–966

Shi Y K, Liu J R, Yang X N, Zhu L M (2009). Fusulinid faunas from the Datangian to Chihsian strata of the Zongdi section in Ziyun county, Guizhou province. Acta Micropalaeontologica Sin, 26(1): 1–30

Smith L B, Read J F (2000). Rapid onset of late Paleozoic glaciation on Gondwana: evidence from Upper Mississippian strata of the Midcontinent, United States. Geology, 28(3): 279–282

Streel M, Caputo M V, Loboziak S, Melo J H G (2000). Late Frasnian-Famennian climates based on palynomorph analyses and the question of the Late Devonian glaciations. Earth Sci Rev, 52(1–3): 121–173

Ueno K, Hayakawa N, Nakazawa T, Wang Y, Wang X D (2013). Pennsylvanian-Early Permian cyclothemic succession on the Yangtze carbonate platform, South China. Geol Soc Lond Spec Publ, 376(1): 235–267

Veever J J, Powell C M (1987). Late Paleozoic glacial episodes in Gondwanaland reflected in transgressive-regressive depositional C sequences in Euramerica. Geol Soc Am Bull, 98(4): 475–487

Wang J S, Jiang G Q, Xiao S H, Li Q, Wei Q (2008). Carbon isotope evidence for widespread methane seeps in the ca. 635 Ma Doushantuo cap carbonate in South China. Geology, 36(5): 345–350

Wang X D, Qie W K, Sheng Q Y, Qi Y P, Wang Y, Liao Z T, Shen S Z, Ueno K (2013). Carboniferous and Lower Permian sedimentological cycles and biotic events of South China. Geol Soc Lond Spec Publ, 376(1): 33–46

Wynn T C, Read J F (2007). Carbon-oxygen isotope signal of Mississippian slope carbonates, Appalachians, USA: a complex response to climate-driven fourth-order glacio-eustasy. Palaeogeogr Palaeoclimatol Palaeoecol, 256(3–4): 254–272

Yang X N (1989). The fusulinids zonation of Maping Formation in Yishan county, Guangxi autonomous region. Geoscience, 3(3): 297–307

Zhang L X, Zhou J P, Sheng J Z (2010). The Upper Carboniferous and Lower Permian Fusulinids from west Guizhou. Beijing: Science Press

Zhou J P (1991). Fusulinid zones from Maping Formation of Changmo, Longlin, Guangxi on Carboniferous–Permian boundary. Acta Palaeontologica Sin, 30(3): 396–409